Interpolating the gravity field using full tensor gradient measurements

Gary Barnes,[1] champions the interpolative power of full tensor gradient (FTG) measurements and its key role in helping oil and gas explorations achieve a better representation of the anomaly field and a clearer picture of the subsurface.

When a gravity or gradiometry survey is performed over an area with ideal sampling and low noise, then in theory, any component is as good to measure as another. The only information lost between different components will relate to constants of integration representing the background field which is often of little interest to the explorationist. In reality, however, the sampling in a survey is often dictated by operational and financial considerations which can ultimately lead to a compromise away from the ideal sampling theorem.

When the distance between measurement points is greater than the shortest half-wavelength signal, the anomaly field will not be adequately sampled. In some cases, small near-surface localized anomalies that lie in between survey lines could even be missed altogether. More commonly, sub-optimal sampling leads to aliasing errors and ultimately problems in interpretation where anomalies can be incorrectly located and oriented. It is in these situations, where the survey line spacing is wide or data coverage is sporadic, that simultaneously measuring multiple components of the gravity gradient tensor becomes highly desirable (Barnes et al., 2008; Brewster, 2011).

In this article, we introduce a simple illustrative model that will show how tensor measurements can be utilized to interpolate and predict the gravity field in between survey lines and ultimately produce a better representation of the anomaly field. The principle will then be demonstrated using data from an actual airborne full tensor gradiometer (FTG) survey.

Tensor components, information content

Figure 1 shows a model consisting of three anomalous masses all with a density contrast of 1 g/cc, together with three associated short survey lines. These lines represent the sampling provided by a widely spaced survey pattern having a high density of sample points along the lines, but sample points only every 2 km across the lines (tie-lines are often even more widely spaced and therefore not considered in this example). Survey line 'A' passes over the centre of a non-rotated block, 'B' passes over a block rotated by 45^0, and 'C' passes alongside a block. These objects are simplistic, but can be thought of as forming the building blocks of more elaborate sources.

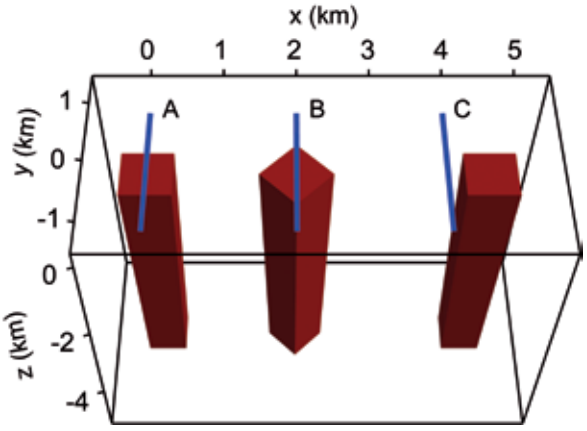

Figure 1 *Model consisting of three anomalous masses (red blocks) and three survey lines (blue lines).*

To illustrate the extra information contained within different components, consider the two lines labelled A and C in Figure 1. Figure 2 shows the G_{zz} and G_{xz} components of the gravity gradient tensor as would be measured along these survey lines. At this stage, no noise is added to the data since we are only considering the affects of sampling and the ability of different tensor components to capture different parts of the anomaly field.

The amplitude of G_{zz} over line C is considerably smaller than that over line A because line C does not pass directly over the source and the component G_{zz} is particularly sensitive to anomalies directly underneath the measurement. The overall shape of the G_{zz} profiles are, however, similar and without extra information this decrease in signal could be misinterpreted as being due to an anomaly directly underneath line C, but with a lower density than the block under line A.

There is insufficient information contained within G_{zz} along this single line to deduce that the block is to the right of survey line C. The component G_{xz}, however, is zero everywhere along survey line A, but shows a positive peak along line C. The absence of signal indicates that the mass

[1] *ARKeX. E-mail: gary.barnes@arkex.com*

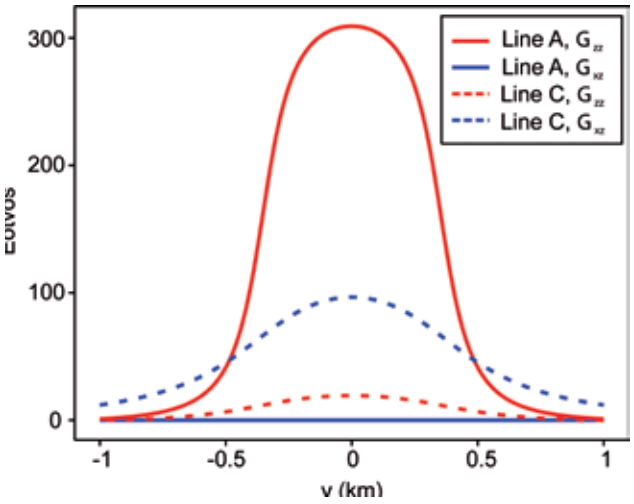

Figure 2 *Tensor components G_{zz} and G_{xz} as measured along lines A and C.*

distribution is symmetrical about line A, but the positive peak indicates that it is increasing in the direction of x for line C. This component is therefore giving anomaly positional information in the x- direction. Each component has its unique use for anomaly discrimination. G_{yz}, for example, would provide positional information along the y- direction, and G_{xx} and G_{yy} help determine the orientation of anomalies and will provide the information to differentiate between the non-rotated and rotated blocks.

Any number of tensor components can be used together in a density inversion that estimates an anomalous mass distribution which explains the data. These inversion problems are ill-posed and require some form of regularization. The most common regularization scheme steers the inversion towards finding the smoothest density distribution that produces fields which fit the measured quantities. This increases the integrity of the inversion and acts to prevent unnecessarily complex solutions.

Figure 3a shows a density distribution where only the G_{zz} component measured along the three survey lines was used as the input data in the inversion. Forward calculations from this density distribution fit the measurements perfectly. Due to the lack of sideways information contained within the G_{zz} component, the inverted anomalous densities tend to be centred underneath the survey lines.

As suggested above, this single, under-sampled component is unable to distinguish between the non-rotated, rotated, and off-centre blocks. In particular, the data from the off-centre block has been inverted to form an anomaly with such a low density contrast that it is barely visible in Figure 3a. The decreased signal amplitude has been explained by a small density contrast directly underneath

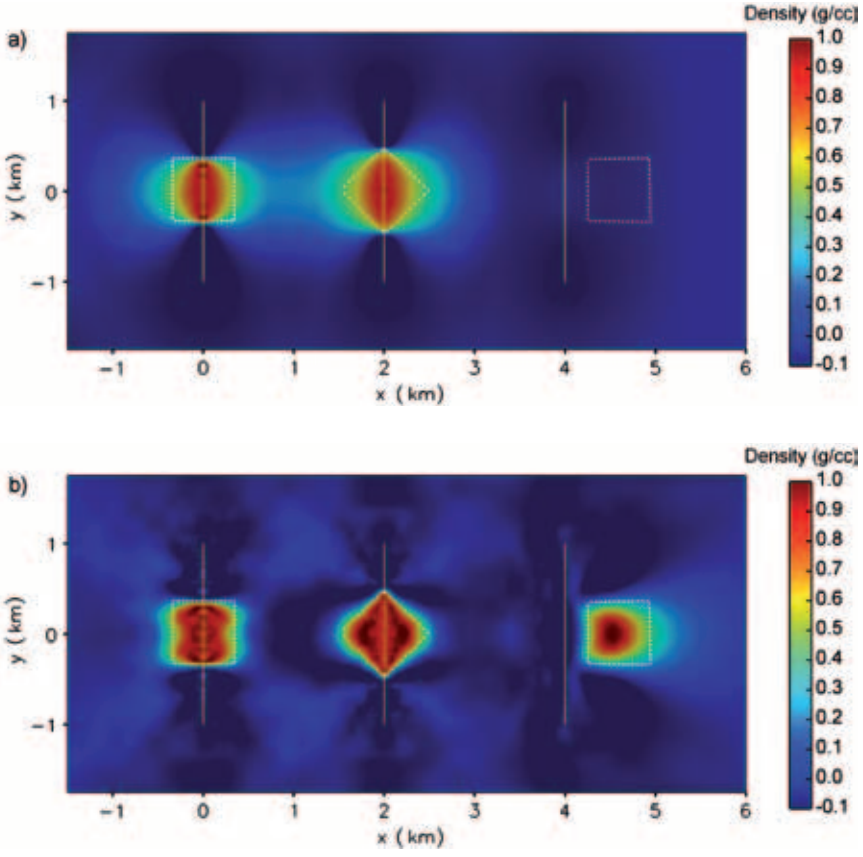

Figure 3 *Density inversions using a) G_{zz} component only and b) full tensor data. Yellow lines represent the three survey lines, dashed outlines show the actual source locations.*

line C. In the presence of a little noise, the anomaly would be basically missed altogether. The rotated nature of the middle block has also been lost and an oval-shaped anomaly has formed.

Figure 3b shows the same type of inversion, but this time utilizing all six tensor components (G_{xx}, G_{xy}, G_{xz}, G_{yy}, G_{yz}, G_{zz}) along the survey lines in a joint density inversion. The result shows that all blocks have been correctly positioned and orientated. Even the third block where the survey line was significantly displaced from the source has been correctly positioned.

Increasing the effective resolution of survey data

The FTG instrument provides six output channels which are the components of differential curvature in a tilted three-axis Cartesian system.

These measurements directly relate to the tensor components and, by forming a complete tensor, can be used to derive all the gravity gradients in any coordinate system on a point-by-point basis.

Bandwidths up to 0.4 Hz are typical in FTG data (equivalent to 75 m half-wavelengths at airborne survey speeds) meaning that the resolution of the data along the survey lines is often much higher than it is across the lines. Using the information within the tensor components to increase the effective resolution in between the lines is therefore highly desirable to make full use of the high bandwidth data.

Having measurements of the complete tensor also has advantages in terms of processing gravity gradient data since equations can be constructed between the individual components that constrain their behaviour (Pajot et al., 2008). Jointly processing all the measurements together is therefore very effective in reducing noise in the data.

To show how the above ideas actually work in practice, we now consider a real airborne FTG survey conducted over an area with proven subsalt oil and gas fields. This data set is ideal in illustrating the advantages of acquiring multiple tensor information because it contains localised high-frequency anomaly signals originating from shallow salt bodies. Such sources provide different information content across the tensor components similar to the earlier illustration.

The survey was performed with a 150 m line spacing, necessary to image the finest details of the salt structures and associated near-surface weathering layer. All the data was processed jointly using the equivalent source scheme described by Barnes and Lumley (2011) and resulted in a high-resolution image of the gravity field over this area with excellent signal to noise ratio for the salt anomalies. Once an equivalent source density model has been deduced, it can be used to forward calculate any gravity or gravity gradient component reprojected on to a grid at constant altitude suitable for visual analysis.

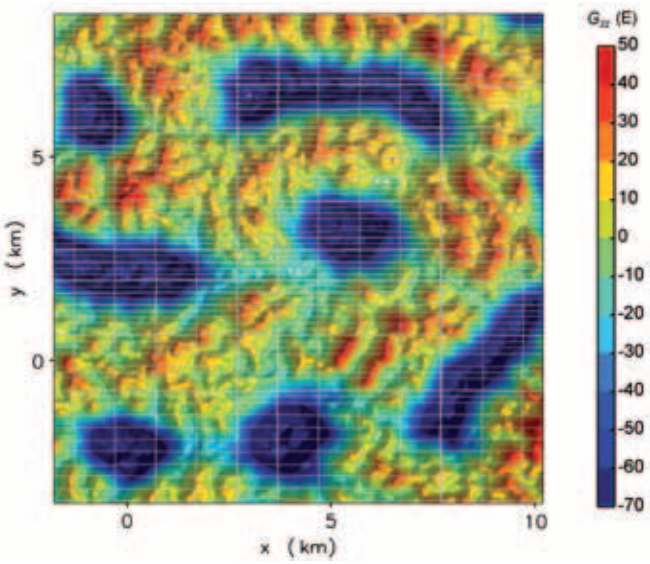

Figure 4 *12 x 12 km section of survey showing G_{zz} deduced from the processing of full tensor data over closely spaced survey lines. Faint grey lines show survey flight lines.*

These forward calculations therefore incorporate all the data from the survey. For qualitative interpretation and presentation, viewing maps of the vertical tensor component, G_{zz}, is often the preferred choice because it shows directly the *x*-*y* locations of anomalous sub-surface density. Figure 4 shows a small (12 x 12) km area of the survey containing seven separate salt bodies. Being a negative density contrast relative to surrounding limestone, the signals from the salt bodies appear as lows in G_{zz} and are therefore easily identified as the blue areas in the graphic.

By selecting flight lines which are separated by roughly 5 km in both directions, a sub-sampled data set can be extracted from the main survey. Processing only the data acquired along these lines will then be used to assess the amount of information that can be recovered using the full tensor measurements from a widely spaced survey. Figure 5 shows the resulting reprojected G_{zz} map where the chosen five flight lines are indicated by the dashed grey lines.

Despite this poor sampling, the basic features (size, shape, orientation, and location) of the salt bodies have been recovered with reasonable integrity. Exactly the same phenomena as shown in the earlier synthetic examples are occurring here.

Each tensor component is providing extra information regarding location and orientation so that when processed together using the equivalent source inversion, the resulting density distribution can be used to more accurately predict the signals in between the original survey lines. The finer details seen in Figure 4 around the salt bodies, however, are lost in this sub-sampled survey result. Many of these features originate from the weathering layer and terrain

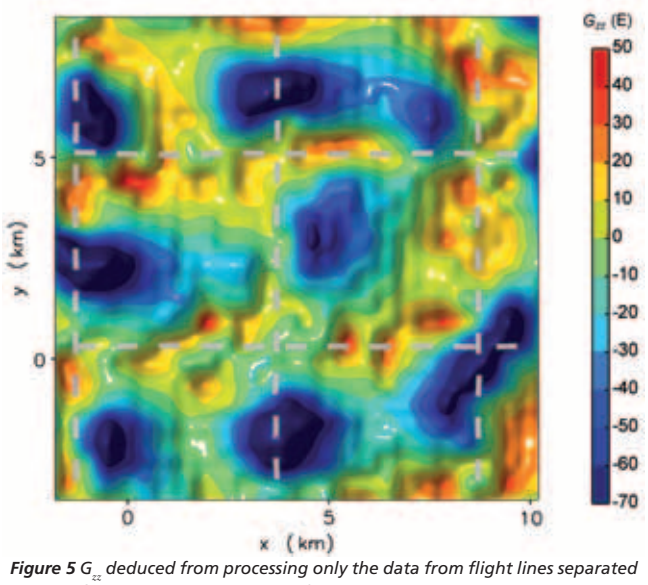

Figure 5 *G_{zz} deduced from processing only the data from flight lines separated by 5 km (shown as gray dashed lines).*

which, although relatively flat, contributed the highest frequency signals.

The ability to interpolate the gravity field between such widely spaced lines can have important consequences for survey planning. One could imagine, for example, a situation where a large area is covered quickly with wide line spacing to identify smaller prospective areas which are subsequently followed up with a series of more detailed surveys.

The result shown in Figure 5 is a slightly special case since the salt bodies, being shallow with a large density contrast (approximately 0.25 g/cc), provide large gravity gradient signals of up to 60 Eotvos. Noise in the data was therefore always sufficiently small to allow clear visibility of the salt signal even along individual survey lines.

A useable spatial resolution of a processed data set can be defined as the bandwidth over which the radial power spectral density (PSD) of the error is less than the PSD of the target signal. Here, the term 'error' means the difference between the perfect signal and the final processed and reprojected data. The error therefore takes into account both the propagation of the noise in the original measurements as well as distortion and potentially poor interpolation, due to the lack of adequate sampling through the survey design.

If we assume that the tightly spaced survey result shown in Figure 4 represents the true G_{zz} field, then the error in the sub-sampled survey can be calculated as the difference between the data in Figures 5 and 4. Analyzing the PSD of this error, Figure 6, then reveals the useable spatial resolution of the sub-sampled data.

Referring to Figure 6, the PSD of the G_{zz} error signal is below the truth signal up to wave-numbers of approximately 3 km^{-1} (equivalent to wavelengths greater than 2 km). Beyond this spatial frequency, the error has a similar level to the signal and suggests that these shorter wavelengths are unresolvable in the processed sub-sampled survey data.

When choosing an appropriate filter to apply to the data in Figure 5, a suitable choice would be a 2 km low-pass filter designed to pass only the part of spectrum where the error is smaller than the signal. When applying this filter to both data sets of Figure 5 and 6, the resulting images look similar, confirming that over this bandwidth the sub-sampled survey is faithfully reproducing the true signal. A wavelength of 2 km therefore defines the useable resolution of this data set, a value less than half the survey line spacing.

Summary

The interpolative power of FTG measurements is playing a key role in helping oil and gas explorations achieve a better representation of the anomaly field and a clearer picture of the subsurface. Applications range from frontier exploration to augmenting existing data sets such as 2D seismic to produce more accurate 3D models of the geology.

By measuring all the components of the gravity gradient tensor, the ability to interpolate or predict the variation of the field in between the survey lines can be greatly improved. This gives rise to an increased effective resolution of an airborne survey which is significantly better than that suggested by the line spacing. The key to the improvement is through joint processing where the information from the tensor components is combined to give a more complete picture of the gravity field. Our preferred method of achieving this is through an equivalent source density inversion which can accommodate any number of components measured at arbitrary locations. The resulting density distribution can subsequently be used to predict

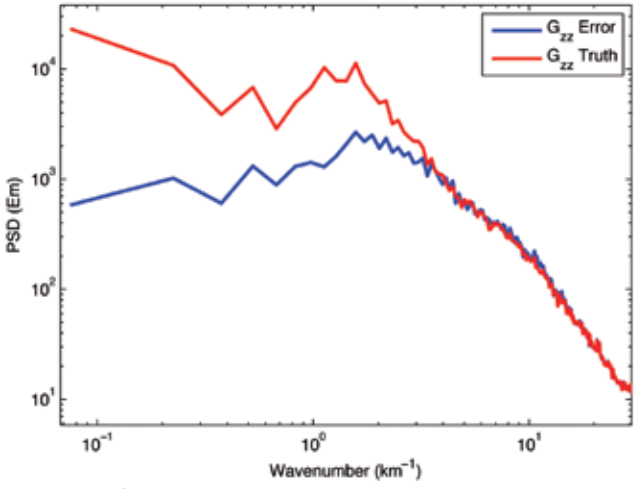

Figure 6 *PSDs for G_{zz} error and truth signal.*

components of the gravity and gravity gradient fields in between the original measurement locations by means of forward calculations.

In the field example, it was shown that collecting full tensor data along flight lines with 5 km spacing could be processed to yield a data set with a useable average radial resolution down to 2 km wavelengths. This Figure is much less than the Nyquist limit of 9 km suggested by the line spacing (Pedersen and Rasmussen, 1990). The increased level of effective resolution was sufficient to image the signal from salt structures that had a width of approximately 2.5 km.

The signal from the salt structures had a large amplitude and therefore provided ample signal to noise ratio even when only the data along the widely spaced survey lines were used. In other cases, the target signals can be much smaller and the line spacing is limited by the need to accurately measure the anomalous field in the presence of noise. This could be referred to as a detectability requirement and drives the line spacing down to produce a useable resolution that has sufficient bandwidth where the signal is above the noise. The enhanced effective spatial resolution resulting from multiple tensor measurements will then be superfluous as a high sampling resolution will already be provided by the survey pattern. In these cases, measuring a single component with a greater signal to noise ratio would be more beneficial. When signal to noise ratio is not the limiting factor, FTG measurements can be used to increase the line spacing without sacrificing resolution and therefore ultimately reduce the cost of a survey.

References

Barnes, G.J., Barraud, J. Lumley, J.M. and Davies, M. [2008] Advantages of multi-tensor high resolution gravity gradient data. *SEG Annual Meeting*, Expanded Abstracts, **28**, 3587–3590.

Brewster, J. [2011] Description and evaluation of a full tensor interpolation method. *SEG Annual Meeting*, Expanded Abstracts, **30**, 344–347.

Barnes, G. J., and Lumley, J.M. [2011] Processing gravity gradient data: *Geophysics*, **76**(2), I33–I47.

Pajot, G., de Viron, O., Diament, M., Lequentrec-Lalancette, M.-F. and Mikhailov, V. [2008] Noise reduction through joint processing of gravity and gravity gradient data. *Geophysics*, **73**(3), 123–134.

Pedersen, L.B. and Rasmussen, T.M. [1990] The gradient tensor of potential field anomalies: Some implications on data collection and data processing of maps. *Geophysics*, **55**(12), 1558–1566.